X-ray absorption and magnetic circular dichroism of $LaCoO_3$, $La_{0.7}Ce_{0.3}CoO_3$, and $La_{0.7}Sr_{0.3}CoO_3$ films: Evidence for cobalt-valence-dependent magnetism

M. Merz,[1,*] P. Nagel,[1] C. Pinta,[1,2] A. Samartsev,[1,3] H. v. Löhneysen,[1,3] M. Wissinger,[1,2] S. Uebe,[1,2] A. Assmann,[1,2] D. Fuchs,[1] and S. Schuppler[1]

[1]*Institut für Festkörperphysik, Karlsruhe Institute of Technology, 76021 Karlsruhe, Germany*

[2]*Fakultät für Physik, Karlsruhe Institute of Technology, 76031 Karlsruhe, Germany*

[3]*Physikalisches Institut, Karlsruhe Institute of Technology, 76031 Karlsruhe, Germany*

(Received 8 September 2010; published 11 November 2010)

Epitaxial thin films of undoped $LaCoO_3$, of electron-doped $La_{0.7}Ce_{0.3}CoO_3$, and of hole-doped $La_{0.7}Sr_{0.3}CoO_3$ exhibit ferromagnetic order with a transition temperature $T_C \approx 84$ K, 23 K, and 194 K, respectively. The spin-state structure for these compounds was studied by soft x-ray magnetic circular dichroism and by near-edge x-ray absorption fine structure at the Co $L_{2,3}$ and O K edges. It turns out that superexchange between Co^{3+} high-spin and Co^{3+} low-spin states is responsible for the ferromagnetism in $LaCoO_3$. For $La_{0.7}Ce_{0.3}CoO_3$ the Co^{3+} ions are in a low-spin state and the spin and orbital moments are predominantly determined by a Co^{2+} high-spin configuration. A spin blockade naturally explains the low transition temperature and the insulating characteristics of $La_{0.7}Ce_{0.3}CoO_3$. For $La_{0.7}Sr_{0.3}CoO_3$, on the other hand, the magnetic moments in the epitaxial films originate from high-spin Co^{3+} and high-spin Co^{4+} states. Ferromagnetism is induced by t_{2g} double exchange between the two high-spin configurations. For all systems, a strong magnetic anisotropy is observed, with the magnetic moments essentially oriented within the film plane.

DOI: 10.1103/PhysRevB.82.174416 PACS number(s): 75.70.−i, 61.05.cj, 71.30.+h, 78.20.Ls

I. INTRODUCTION

Transition-metal oxides with strong electronic correlations have long been known for their unusual electronic and magnetic phenomena, frequently posing fundamental challenges for our understanding of condensed matter: high-temperature superconductivity in cuprates or colossal magnetoresistance and complex orbital ordering in manganites are but a few examples. Spearheaded by superconducting $Na_xCoO_2 \cdot yH_2O$ (Ref. 1) and by magnetoresistive and orbital ordering effects in $RBaCo_2O_{5+x}$,[2–4] cobaltates have recently emerged as a further center of interest. They are distinguished and even unique in that they offer an additional and possibly tunable aspect—the spin degree of freedom.

Among the many competing interactions occurring on similar energy scales (e.g., Hund's coupling, crystal field, double exchange, and correlation), the spin degree of freedom is essentially determined by a delicate balance between the crystal-field splitting Δ_{CF}, i.e., the energetic splitting between t_{2g} and e_g orbitals, and the exchange interaction J_{ex} associated with Hund's rule coupling. Depending on the relative values of Δ_{CF} and J_{ex}, electrons are redistributed between t_{2g} and e_g levels and for a Co^{3+} ion three spin configurations are being discussed:[5] a low-spin state (LS, $t_{2g}^6 e_g^0$, $S=0$), a high-spin state (HS, $t_{2g}^4 e_g^2$, $S=2$), and an intermediate-spin state (IS, $t_{2g}^5 e_g^1$, $S=1$); yet in the case of bulk $LaCoO_3$ (LCO) the existence of an IS state is still under debate.[6–20] In any case, there is general agreement that for $T \to 0$, Co^{3+} in bulk $LaCoO_3$ goes to an LS state (except for Curie-Weiss-type impurity contributions).

In a previous work it was reported that in contrast to bulk material, epitaxial thin films of $LaCoO_3$ become ferromagnetic below a Curie temperature, T_C, of 85 K while polycrystalline thin films grown under similar conditions behave like the bulk material where no indication for ferromagnetism is found down to 5 K.[21] It was also demonstrated that epitaxial thin films do not show any significant spectral changes in near-edge x-ray absorption fine structure (NEXAFS) for temperatures between 30 and 450 K, implying that the spin state remains constant and that the tensile strain inhibits any increase in the LS-state population with decreasing temperature.[22] Alternatively, ferromagnetic order can also be induced in $LaCoO_3$ by partial replacement of La^{3+} by Ce^{4+} or by Sr^{2+}. A 30% substitution by Ce^{4+} leads to a T_C of 22 K while for 30% Sr^{2+} a T_C up to 240 K is found.[23,24] This strongly "asymmetric" doping-dependent behavior of T_C is in contrast to what is found for other transition-metal oxides like the manganites: in the case of the Mn $t_{2g}^3 e_g^{1\pm x}$ configuration an equivalent amount of electron or hole doping leads to a comparable change in T_C. For the manganites it was further shown that, irrespective of the type of doping, ferromagnetic ordering is always induced by the double-exchange mechanism.[25]

In the case of the perovskite cobaltates, doping and epitaxial strain usually modify the Co-O-Co bond angles and the Co-O bond lengths. Since Δ_{CF} is strongly affected by changes in the Co-O bond lengths, the balance between Δ_{CF} and J_{ex} can easily be influenced by epitaxial strain and (electron/hole) doping, leading to a tunable spin configuration. Of course, strain and doping effects may coexist for doped thin films.

To elucidate the mechanisms leading to the magnetic properties in the cobaltates we compare the NEXAFS and the soft x-ray magnetic circular dichroism (SXMCD) of epitaxially strained LCO, of electron-doped $La_{0.7}Ce_{0.3}CoO_3$ (LCCO), and of hole-doped $La_{0.7}Sr_{0.3}CoO_3$ (LSCO). The spectra establish that due to completely different spin configurations, ferromagnetism has a different origin in strained LCO (superexchange) and hole-doped LSCO (double exchange). On the other hand, electron-doped LCCO poses one

of the rare cases where the spin configuration on neighboring Co^{3+} and Co^{2+} sites leads to an insulating spin blockade. The results of the current study give a natural explanation for the strong discrepancy found for T_C between electron- and hole-doped perovskite cobaltates and directly explain why the cobaltates behave so differently compared to other transition-metal oxides like the manganites. Using the established XMCD sum rules,[26–28] estimates for the spin and orbital contributions of the magnetic moments are determined. A clear anisotropy with the spin and orbital moments predominantly lying within the film plane is found for all investigated $La_{1-x}A_xCoO_3$ (A=Ce,Sr) samples.

II. EXPERIMENTAL

All film samples were grown on ⟨001⟩ oriented 0.1% Nb-doped $SrTiO_3$ (Nb:STO) substrates by pulsed laser deposition using stoichiometric sinter targets of the corresponding compound. Film thickness was about 50 nm. The growth conditions were the same as those reported in Refs. 21–24 and 29. The samples were characterized by x-ray diffraction and by superconducting quantum interference device (SQUID) magnetometry. The T_C values and saturated magnetic moments are summarized in Table I. Using the setup of the Max-Planck Institute for Metals Research (Stuttgart, Germany) SXMCD measurements were performed at 20 K in total electron yield and with an applied magnetic field of ±2 T at the Institut für Festkörperphysik beamline WERA at the ANKA synchrotron light source (Karlsruhe, Germany). All spectra were measured with circularly polarized light, and NEXAFS spectra were obtained by averaging the two spectra taken with the projection of the photon spin parallel (μ^+ spectrum) and antiparallel (μ^- spectrum) to the spin of the Co majority electrons. From the hysteresis loops of the investigated samples it was evident that the magnetic moments were all saturated around 1 T, i.e., significantly below the 2 T used for the SXMCD experiment. The energy resolution of the absorption spectra was set to 0.3 eV for the Co $L_{2,3}$ edge and to 0.15 eV for the O K edge. To study $\vec{B}\|\vec{n}$ and $\vec{B}\perp\vec{n}$ anisotropies, spectra were taken at normal incidence [$\varphi=\sphericalangle(\vec{n},-\vec{k})=0°$] and at grazing incidence ($\varphi=65°$), where $\vec{B}$ is the magnetic field, $\vec{n}$ the surface normal of the sample, and $\vec{k}$ the propagation vector of light. $\vec{B}\perp\vec{n}$ values are derived by extrapolating φ to 90°.[30] After correction for photon-flux variations and for the background, the spectra were normalized at the edge jump, and the finite degree of circular polarization (0.85) was taken into account. Photon-energy calibration was ensured by adjusting the Ni L_3 peak position measured on a NiO single-crystal before and after each NEXAFS/SXMCD scan to the established peak position.[31]

TABLE I. Transition temperature, T_C, and saturated magnetic moment, μ_{sat}, at 20 K for LCO, LCCO, and LSCO as determined from magnetometry.

	LCO	LCCO	LSCO
T_C (K)	84	23	194
μ_{sat} (20 K) (μ_B/Co)	0.85	0.21	0.88

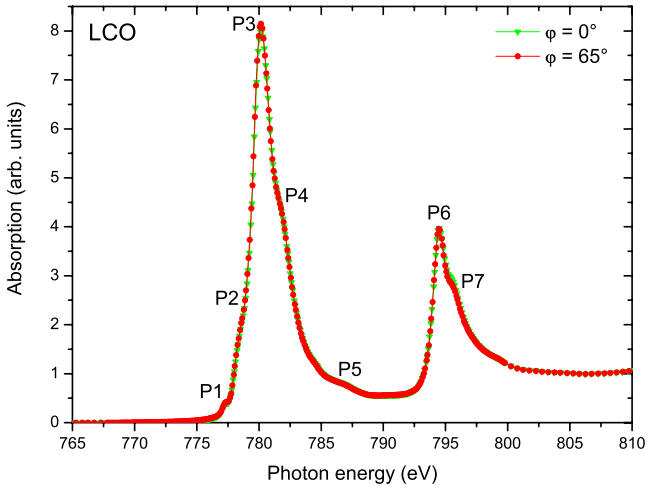

FIG. 1. (Color online) $\varphi=0°$ and $\varphi=65°$ Co $L_{2,3}$ NEXAFS spectra of LCO taken at 20 K. No spectral changes occur with sample orientation, reflecting the isotropic nature of the unoccupied electronic density of states.

III. RESULTS AND DISCUSSION

A. Co $L_{2,3}$ NEXAFS

As a representative for all investigated $La_{1-x}A_xCoO_3$ (A=Ce,Sr) samples, Fig. 1 shows the in-plane and out-of-plane Co $L_{2,3}$ NEXAFS spectra of LCO measured at 20 K.[32] The LCO absorption spectra correspond in first order to transitions of the type Co $2p^63d^n \rightarrow$ Co $2p^53d^{n+1}$ (n=6 for Co^{3+}). They consist of two manifolds of multiplets situated around 780 eV (L_3) and 795 eV (L_2) and separated by the spin-orbit splitting of the Co $2p$ level. The features at both edges resemble those of a typical Co^{3+} low-spin system like $EuCoO_3$.[33] For all spectra a small spectral Co^{2+} contribution centered at 777.4 eV (feature P1) is present which can be attributed to some residual oxygen deficiency as discussed below. The present LCO absorption data reproduce the measurements published in Ref. 22. No spectral changes are found for the $La_{1-x}A_xCoO_3$ samples between the $\varphi=0°$ and $\varphi=65°$ Co $L_{2,3}$ absorption spectra. This, on the one hand, reflects the homogeneity of the samples and the isotropic nature of the unoccupied electronic density of states. On the other hand, it shows that in $La_{1-x}A_xCoO_3$ the Co absorption is not dominant enough to cause a discernible role of saturation effects as described in Refs. 34 and 35. These effects can thus be neglected.

In Fig. 2 the $\varphi=0°$ Co L_3 absorption spectra of LCO, LSCO, and LCCO are compared.[32] The inset shows the corresponding L_2 edges. At both edges, changes in the spectral shape are observed upon electron/hole doping: When going from LCO to LCCO, spectral weight (SW) is transferred from the main L_3 peak at 780.2 eV (P3) and the two high-energy shoulders around 782 eV (P4) and 786.2 eV (P5) to the peaks/shoulders on the low-energy side at 777.4 eV (P1) and at 778.6 eV (P2). The labeling of the features is given in

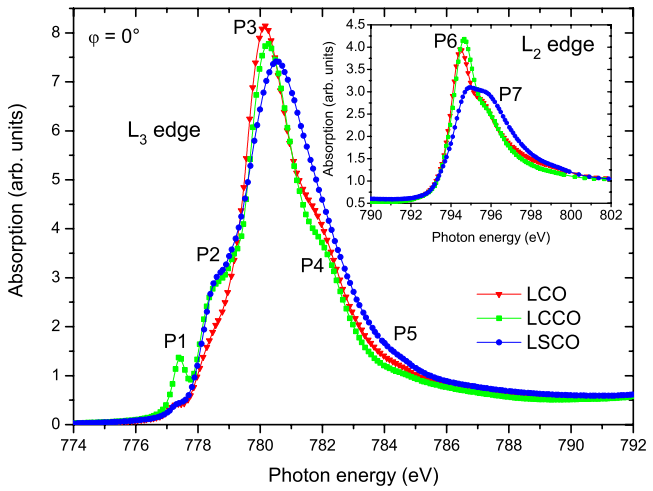

FIG. 2. (Color online) Comparison of the $\varphi=0°$ Co L_3 NEXAFS spectra of LCO, LCCO, and LSCO taken at 20 K. The inset shows the corresponding L_2 spectra. The spectral shape of both edges changes upon doping.

Figs. 1 and 2. At the L_2 edge only a rather small transfer of spectral weight from shoulder P7 to peak P6 is observed, indicating that the LS state remains the dominant spin configuration of Co^{3+} upon 30% electron doping. When going from LCO to LSCO, the spectral weight of P3 decreases while features P2, P4, and P5 increase. Moreover, P3 shifts to slightly higher energies. At the L_2 edge, P6 is strongly reduced while feature P7 grows, thereby strongly changing the spectral shape of this edge. Already at first sight it is evident from comparison with other LS systems that Co^{3+} LS states do not play the same prominent role in LSCO as they do in LCO. As will be shown, the observed change in the spectral shape indicates that upon Sr doping, the Co^{3+} LS configuration is to a large extent replaced by Co^{4+} HS.

The spectra can be qualitatively analyzed in more detail using atomic multiplet plus crystal-field calculations. The code developed by Thole[36–38] and maintained and further developed by de Groot[39–41] was used to calculate spectra for different values of the crystal-field splitting Δ_{CF} and of the charge-transfer energy Δ_c. Charge-transfer effects were included for Co^{3+} by admixing transitions of the type $2p^63d^7\underline{L}\rightarrow 2p^53d^8\underline{L}$, where $\underline{L}$ denotes a hole in the oxygen ligand. Correspondingly, $2p^63d^8\underline{L}\rightarrow 2p^53d^9\underline{L}$ and $2p^63d^6\underline{L}\rightarrow 2p^53d^7\underline{L}$ transitions were admixed for Co^{2+} and Co^{4+}, respectively. All multiplet calculations were performed for an octahedral O_h symmetry. The Slater integrals were renormalized to 80% of their Hartree-Fock values to approximately account for intra-atomic configuration interactions. To compare the calculated data with the experiment, a Lorentzian broadening with $\sigma=0.2$ eV ($\sigma=0.3$ eV) and a Gaussian broadening with $\sigma=0.3$ eV were applied to the L_3 (L_2) edge to approximately account for lifetime, phononic, and resolution effects. Figure 3 shows the calculated Co $2p$ XAS spectra of Co^{3+} LS, Co^{3+} HS, Co^{3+} IS, Co^{2+} HS, Co^{4+} LS, and Co^{4+} HS. (The spectra for Co^{2+} LS and for Co^{4+} IS are not considered since a Co^{2+} LS state is induced only by strong Jahn-Teller distortions and a Co^{4+} IS state is stabilized only in case of strong negative charge-transfer effects.) The

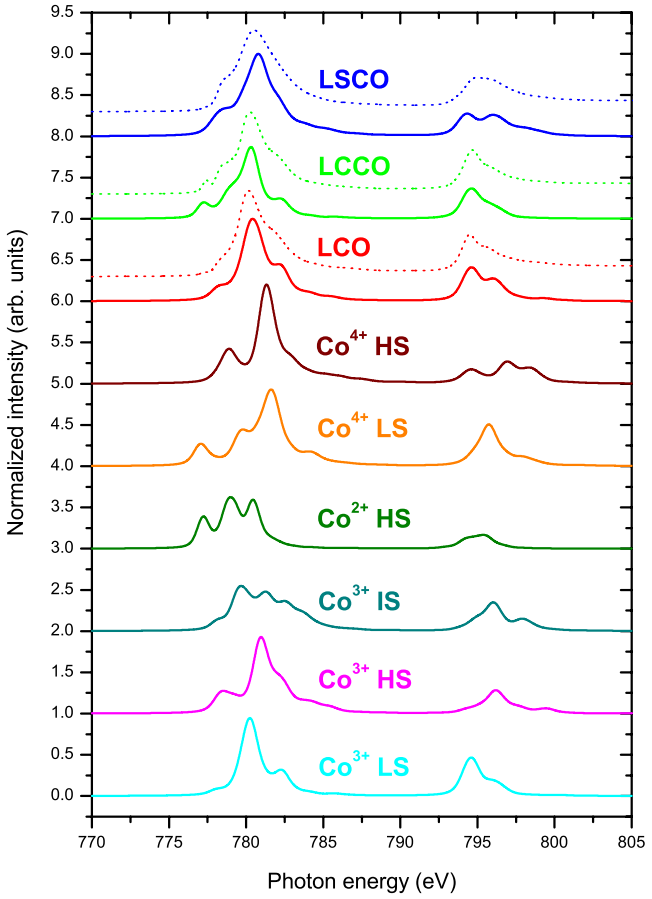

FIG. 3. (Color online) Co $2p$ XAS multiplet calculations of Co^{3+} LS, Co^{3+} HS, Co^{3+} IS, Co^{2+} HS, Co^{4+} LS, and Co^{4+} HS. In addition the simulated (solid line) and measured (dotted line) spectra of LCO, LCCO, and LSCO are also depicted. For clarity, the spectra for the different configurations are offset.

calculated spectra are similar to previous multiplet calculations.[16,22,42–44] It has been established previously that the Co^{3+} IS configuration is not stable for the O_h symmetry of the CoO_6 octahedron in LCO.[16,22] Yet for completeness, we have included a Co^{3+} IS spectrum (calculated for a tetragonal D_{4h} symmetry) in Fig. 3 as well. Its spectral shape clearly demonstrates that it cannot be a significant species in the systems under study here. In addition the simulated and measured spectra of LCO, LCCO, and LSCO are also depicted. The simulated spectra are obtained for appropriate linear combinations of calculated spectra for single configurations. The shapes of the simulated spectra strongly depend on the crystal field, charge transfer, spin-orbit coupling, intra-atomic configuration interactions, energetic position, and other parameters. For a discussion of the valence and spin state of the Co ions, the simulations depicted in Fig. 3 reproduce fairly well all major features of the experimental results. While it was not attempted to obtain a one-to-one equivalence between the measured and the simulated data by fine adjustment of all fitting parameters, it is satisfying to note that the parameters chosen reproduce the measured data at both the L_3 and the L_2 edges.

The simulations clearly show that the spectral shape of LCO in Fig. 2 is dominated by low-spin Co^{3+}. The elaborate

fitting procedure used in Ref. 22 has already shown that the spectral shape of LCO is correctly described by a mixture of ≈64% Co^{3+} LS and ≈36% Co^{3+} HS. This result is in agreement with the current data. The LCCO spectrum is dominated by the features of Co^{3+} LS as well. Yet the spectral features of the L_3 edge, i.e., the peak at 777.4 eV (P1) and the shoulder around 778.6 eV (P2), unambiguously corroborate the presence of Co^{2+} HS expected for an electron-doped system. The changes observed at the $L_{2,3}$ edges, as described above, together with the multiplet calculations suggest that corresponding to the doping content, Co^{2+} replaces ≈30% Co^{3+} HS when going from LCO to LCCO. Any remaining contribution of Co^{3+} HS, if present, is too small to be identified in the NEXAFS data, and we obtain a 30% Co^{2+} HS/70% Co^{3+} LS configuration for LCCO. For LSCO, on the other hand, the changes in the spectral features at the L_3 and especially the more pronounced variations at the L_2 edge suggest a replacement of Co^{3+} LS by Co^{4+} HS while the amount of Co^{3+} HS remains comparable to that in LCO: As can be inferred from the simulations, the spectral shape of both edges indicates a mixture of about 40% Co^{3+} HS, 30% Co^{3+} LS, and 30% Co^{4+} HS. Even though the experimental spectrum of LSCO can be simulated quite well using this combination of charge and spin states, Co^{4+} IS configurations (i.e., $\alpha'|d^6\rangle+\beta'|d^7\underline{L}\rangle$ states) cannot completely be ruled out at this time. For LSCO the issue of IS states becomes even more important since the Co^{4+} ion seems to be in an IS state in $SrCoO_3$.[45] In the context of the oxygen edge, however, it will be demonstrated that this is not the case for our thin-film samples.

Regarding the small oxygen deficiency mentioned above, we note that feature P1, an indicator for Co^{2+}, is present in all spectra, cf. Fig. 2. Although this Co^{2+} contribution had been minimized by optimizing growth conditions it could not be completely avoided. The identical spectral weight of P1 for LCO and LSCO (corresponding to ≈5% Co^{2+}) suggests that *all* investigated systems (including LCCO) are slightly oxygen deficient.

B. Co $L_{2,3}$ SXMCD

Figure 4 shows the SXMCD spectra ($\Delta\mu=\mu^+-\mu^-$) of LCO taken at 20 K.[32] In contrast to the corresponding NEXAFS spectra, a clear anisotropy is found between normal- and grazing-incidence SXMCD data. Compared with the $\varphi=0°$ spectrum, the $\varphi=65°$ spectrum has a much higher intensity and also significantly different spectral features: A distinct negative double peak is found in the $\varphi=65°$ data with feature A around 778.1 eV and feature B at 780.0 eV while feature C around 778.9 eV followed by a slightly broader negative peak at ≈780.1 eV (feature D) appears for the $\varphi=0°$ spectrum. Moreover, the SXMCD signal at the L_2 edge is almost absent in the $\varphi=0°$ data. This strong anisotropy already illustrates that the easy axis and the magnetic moments of LCO lie predominantly within the film plane. Interestingly, a small upturn (feature E) is found in the $\varphi=0°$ spectrum around 777.4 eV. This is exactly the energy range of peak P1 in Figs. 1 and 2. Therefore, this upturn can be attributed to a small amount of magnetically active Co^{2+} in LCO due to a slightly reduced oxygen content as already inferred from the NEXAFS data above. On the other hand, feature E seems to be completely compensated in the $\varphi=65°$ spectrum by the strong spectral weight (SW) of feature A and, thus, no indications for oxygen deficiency appear in the $\varphi=65°$ data. Taken together, the data shown in Fig. 4 point to a negligibly small contribution of the oxygen-deficiency-induced Co^{2+} to the *total* SXMCD SW in the LCO sample, and it is evident that the magnetic moment in LCO is essentially determined by Co^{3+} HS states.

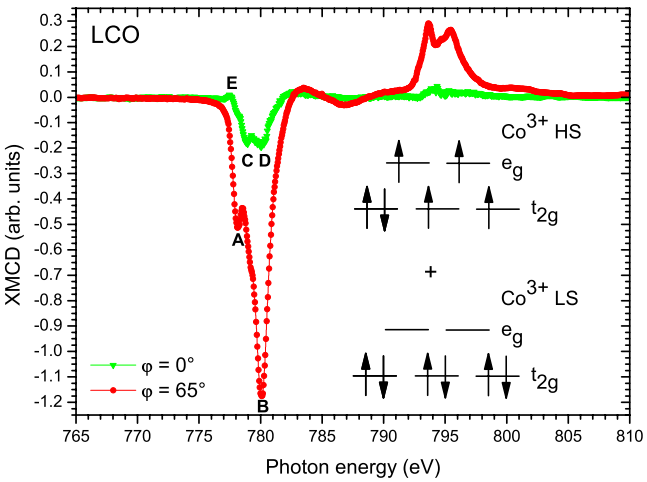

FIG. 4. (Color online) $\varphi=0°$ and $\varphi=65°$ Co $L_{2,3}$ SXMCD spectra of LCO taken at 20 K. A clear anisotropy between normal and grazing incidence is found. The magnetic moments are essentially caused by high-spin Co^{3+} states.

Estimates for the spin (m_{spin}) and the angular-dependent orbital contributions (m_{orb}^{φ}) of the magnetic moments can be derived using the established XMCD sum rules[26–28,30,46–48]

$$m_{orb}^{\varphi}=-4\frac{(\Delta A_{L_3}+\Delta A_{L_2})_{\varphi}}{3(A_{L_3}+A_{L_2})}n_h, \tag{1}$$

$$m_{eff}=m_{spin}+7m_T^{\varphi}=-\frac{(2\Delta A_{L_3}-4\Delta A_{L_2})_{\varphi}}{A_{L_3}+A_{L_2}}n_h, \tag{2}$$

where m_{orb}^{φ}, m_{spin}, the effective spin moment m_{eff}, and the angular-dependent magnetic dipole moment m_T^{φ} are in units of μ_B/atom, $n_h=10-n_{3d}$, with n_{3d} being the $3d$ electron occupation number, ΔA_{L_3} and ΔA_{L_2}, and A_{L_3} and A_{L_2} are the XMCD and NEXAFS intensities integrated over the L_3 and L_2 edges, respectively. It has been shown that the magnetic dipole term in the spin sum rule can be separately determined in an angle-dependent XMCD measurement.[30,46] For $3d$ electron systems the angular average of m_T^{φ} vanishes and one can write

$$m_T^{\perp}+2m_T^{\parallel}=0 \tag{3}$$

and calculate both the intra-atomic dipole components m_T^{φ} and the spin moment m_{spin}.[30,46] The in-plane dipole component $m_T^{\parallel}$ is obtained from the measured components $m_T^{\perp}$ and m_T^{φ} according to

$$m_T^{\varphi} = m_T^{\perp} \cos^2 \varphi + m_T^{\parallel} \sin^2 \varphi. \quad (4)$$

Similarly, the in-plane orbital moment $m_{orb}^{\parallel}$ is related to the measured components $m_{orb}^{\perp}$ and m_{orb}^{φ} according to

$$m_{orb}^{\varphi} = m_{orb}^{\perp} \cos^2 \varphi + m_{orb}^{\parallel} \sin^2 \varphi. \quad (5)$$

Furthermore, the transition-metal correction factors for the spin sum rule caused by Coulomb interaction (mixing of the L_3 and L_2 region) were applied.[49] The values deduced in this way for LCO are shown in Table II. In a uniaxial system, the spin-orbit-induced energy anisotropy, ΔE_{SO}, is directly linked to the anisotropy of the orbital moment,[50] and for a more than half-filled $3d$ shell one obtains[46]

$$\Delta E_{SO} \sim -(m_{orb}^{\perp} - m_{orb}^{\parallel}). \quad (6)$$

The moments given in Table II and especially the negative value of $\Delta_{orb} = m_{orb}^{\perp} - m_{orb}^{\parallel}$ ($m_{orb}^{\parallel} > m_{orb}^{\perp}$) reflect the strong magnetic anisotropy of the sample, with the orbital moment and, as a consequence of the spin-orbit coupling, also the spin predominantly residing within the film plane. Employing a single-ion model where $m_{spin} \approx 2 \cdot \langle S_z \rangle \mu_B$/Co, the measured spin moment of 0.77(1) μ_B/Co corresponds to ≈19% of Co^{3+} in an HS state. The value of the spin moment is consistent with the 0.85 μ_B/Co found in our SQUID measurements for the saturated moment on LCO. At first sight, the finding of ≈19% of Co^{3+} in an HS configuration seems to be in contrast to the ≈36% in an HS state deduced from the NEXAFS results. The numbers are, however, fully compatible if one considers the microscopic situation that may well be described in analogy to percolative effects: If the Co^{3+} HS states are distributed statistically in the Co^{3+} LS matrix only a fraction of them will be arranged together with the LS species in the required long-range three-dimensional checkerboardlike manner. As a consequence, only a certain number of clusters with a size sufficient for ferromagnetism will be formed. We will continue the discussion of the spin state in terms of a microscopic picture in the context of the O edge.

TABLE II. Spin moment m_{spin} and spin-density anisotropy $m_T^{\parallel}$ and $m_T^{\perp}$ together with the orbital moments $m_{orb}^{\parallel}$ and $m_{orb}^{\perp}$. $m_T^{\perp}$ and $m_{orb}^{\perp}$ are the out-of-plane moments measured at $\varphi = 0°$ while $m_T^{\parallel}$ and $m_{orb}^{\parallel}$ are the in-plane projected moments calculated from the measured quantities at $\varphi = 0°$ and $\varphi = 65°$ as discussed in Refs. 30 and 46. In addition the averaged orbital moment m_{orb}^{av}, the difference $\Delta_{orb} = m_{orb}^{\perp} - m_{orb}^{\parallel}$, and the ratio m_{orb}^{av}/m_{spin} are given. Errors are shown in brackets (Ref. 48).

	LCO	LCCO	LSCO
m_{spin} (μ_B/Co)	0.77(1)	0.24(2)	0.92(2)
$m_T^{\parallel}$ (μ_B/Co)	−0.042(3)	−0.007(3)	−0.029(3)
$m_T^{\perp}$ (μ_B/Co)	0.084(3)	0.013(2)	0.058(1)
$m_{orb}^{\parallel}$ (μ_B/Co)	0.187(2)	0.117(5)	0.352(4)
$m_{orb}^{\perp}$ (μ_B/Co)	0.039(2)	0.064(3)	0.156(2)
m_{orb}^{av} (μ_B/Co)	0.137(2)	0.101(4)	0.287(3)
Δ_{orb} (μ_B/Co)	−0.148(3)	−0.053(6)	−0.196(4)
m_{orb}^{av}/m_{spin}	0.20(2)	0.46(2)	0.35(2)

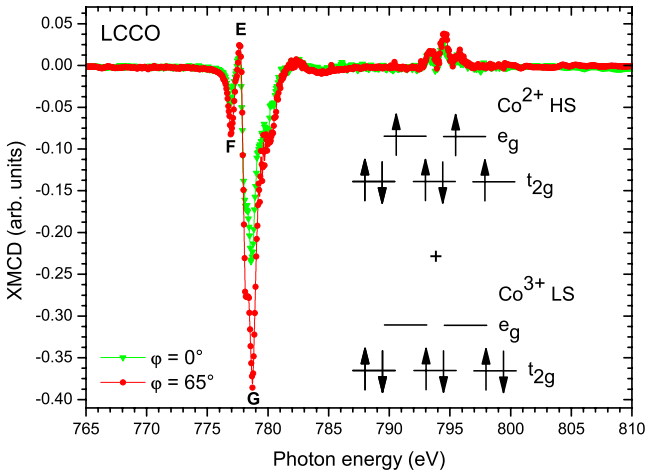

FIG. 5. (Color online) $\varphi = 0°$ and $\varphi = 65°$ Co $L_{2,3}$ SXMCD spectra of LCCO taken at 20 K. In contrast to LCO, a reduced anisotropy between $\varphi = 0°$ and $\varphi = 65°$ spectra is found. The magnetic moments are predominantly determined by Co^{2+}.

In Fig. 5 the $\varphi = 0°$ and $\varphi = 65°$ Co $L_{2,3}$ SXMCD spectra of LCCO are depicted.[32] (Note that the intensity scale is reduced by a factor of ≈3 compared to Fig. 4.) In contrast to LCO, the anisotropy between the $\varphi = 0°$ and $\varphi = 65°$ spectra is reduced for LCCO and the spectral shape is very similar for both angles. Nevertheless, the anisotropy still remaining indicates that the easy axis and the magnetic moments of LCCO preferably reside in the film plane, too. The spectral shape of the LCCO data clearly differs from that of LCO: a conspicuous minimum is now observed at 776.9 eV (feature F) followed by the upturn typical for Co^{2+} (feature E described above). A dominant negative peak is found at ≈778.7 eV (feature G) with a sharp shoulder around 778.2 eV on the low-energy side of the peak and a broad shoulder on the high-energy side. The features at the Co L_2 edge are again quite small. When comparing the main peak at the L_3 edge of LCO and LCCO, a clear shift to lower energies by more than 1.3 eV, i.e., toward the spectral region of Co^{2+} occurs for the latter and the SW in the energy range of the Co^{3+} states is strongly reduced. This, however, is possible only if the Co^{3+} ion is in an LS state (without any contribution to the spin and orbital moments) and if the magnetic moments of LCCO are dominated by Co^{2+} HS. This result is consistent with the 30% Co^{2+} HS/70% Co^{3+} LS configuration concluded from the NEXAFS multiplet simulations. Table II shows estimates for the spin and orbital moments deduced by applying the sum rules. The spin moment of 0.24(2) μ_B/Co determined from the SXMCD data is in agreement with the 0.21 μ_B/Co found at 20 K in our SQUID measurements for the saturated moment on LCCO. With the Co^{2+} HS/Co^{3+} LS configuration found in the SXMCD data, the insulating behavior of the compound is also understandable, as the hopping process of the electron from the Co^{2+} HS to the Co^{3+} LS site is strongly suppressed by a spin blockade similar to that reported in Refs. 44 and 51. It might be speculated that the Co^{2+} HS state (with its large ionic radius) is stabilized by the tensile strain imposed by the substrate and the reduced radius of the Co^{3+} LS state (compared to the Co^{3+} HS ion). In other words, the spin blockade found in the current investigation

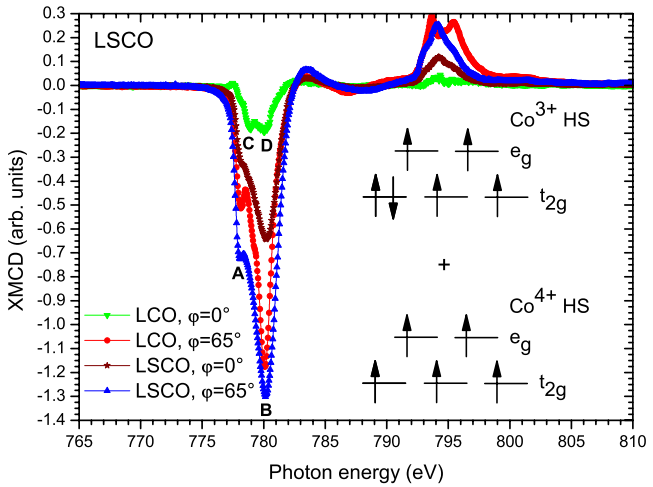

FIG. 6. (Color online) $\varphi=0°$ and $\varphi=65°$ Co $L_{2,3}$ SXMCD spectra of LSCO taken at 20 K. For comparison the $\varphi=0°$ and $\varphi=65°$ Co $L_{2,3}$ data of LCO are included. The magnetic moments are caused by Co^{3+}/Co^{4+} high-spin states.

might be specific only for electron-doped epitaxial films. We note that our LCCO films are so far the only $La_{1-x}Ce_xCoO_3$ samples with significant electron doping.

Figure 6 shows the $\varphi=0°$ and $\varphi=65°$ Co $L_{2,3}$ SXMCD data of LSCO.[32] For comparison, the corresponding spectra of LCO are included. The two LSCO spectra have a very similar spectral shape: both exhibit a negative peak at 780.1 eV (feature B) with a shoulder around 778.0 eV (feature A) on the low-energy side. Hence, the energetic positions of these structures coincide for LSCO and LCO. Yet in contrast to LCO, the L_2 edge of LSCO does not exhibit a double-peak feature any more but rather a single peak at 794.1 eV with a shoulder on the low- and high-energy side. This finding apparently reflects the changes in the valence and in the spin state of the Co ion already discussed in the NEXAFS data of LSCO. For LSCO a strong anisotropy with the magnetic moments lying within the film plane is obvious from the spectra. This is further supported by the estimates for the magnetic moments obtained from the sum rules: again the orbital and spin moment shown in Table II are found to be oriented within the film plane. The spin moment of 0.92(2) μ_B/Co derived from the SXMCD spectra is consistent with the 0.88 μ_B/Co determined for the saturated moment from the SQUID data. Similarly to LCO, however, a much higher magnetic moment would be expected for the 40% Co^{3+} HS, 30% Co^{3+} LS, and 30% Co^{4+} HS configuration deduced from the NEXAFS spectra. The variance might again be attributed to percolative effects. Support comes from neutron diffraction and magnetic-susceptibility investigations on polycrystalline $La_{1-x}Sr_xCoO_3$ where a percolation threshold around 30% was suggested to explain the ferromagnetic metallic behavior of the samples.[52,53]

C. O *K* NEXAFS and SXMCD

In Fig. 7 the $\varphi=65°$ O *K* absorption and SXMCD spectra of LCO, LSCO, and LCCO are compared between 526 and 532 eV.[32] In this energy range the spectra reflect the unoccupied O $2p$ density of states hybridized with Co $3d$ e_g and t_{2g} orbitals. For LCCO a strong peak centered around 530 eV is found in the absorption data. This feature corresponds to a large number of unoccupied states in the e_g area.[22] The states in the t_{2g} area (below 529 eV), on the other hand, are almost completely occupied. This result can be qualitatively understood in terms of a very simplified model where charge transfer between Co and O is neglected and just the number of unoccupied states of the ionic Co e_g and t_{2g} levels (see also inset of Figs. 4–6, respectively) is counted: As an example, for the 70% Co^{3+} LS states both e_g levels are empty in LCCO and the t_{2g} levels are completely filled; for the 30% Co^{2+} HS ions both e_g and one t_{2g} level are half-filled while two t_{2g} levels are occupied. Consequently, this configuration leads to the observed strong SW ($0.7\times4+0.3\times2=3.4$) of the e_g states and a quite small intensity ($0+0.3\times1=0.3$) for the t_{2g} area. The plot associated with the spectral weight of the e_g and the t_{2g} states is depicted in the inset of Fig. 7. Back to the main panel it is obvious that when going to LCO, SW is transferred from the e_g to the t_{2g} range, reflecting a transfer of electrons from t_{2g} to e_g levels. This rearrangement, however, is expected for the 36% Co^{3+} HS (64% Co^{3+} LS) configuration determined for LCO (see inset of Fig. 4). For LSCO, the transfer of SW from the e_g to the t_{2g} range continues: The e_g SW is significantly reduced when going from LCO to LSCO while the t_{2g} SW is considerably increased. Using again our model, the observed transfer of SW is consistent with the 40% Co^{3+} HS, 30% Co^{3+} LS, and 30% Co^{4+} HS mixture determined from the multiplet calculations and the Co $L_{2,3}$ NEXAFS spectra. Thus, the O *K* absorption data corroborate the spin configurations found for LCO, LCCO, and LSCO at the Co $L_{2,3}$ edge.

While this simple model does indeed capture qualitatively the SW changes observed, it is clearly insufficient to examine possible Co^{3+} and Co^{4+} IS states:[54] to further discuss IS

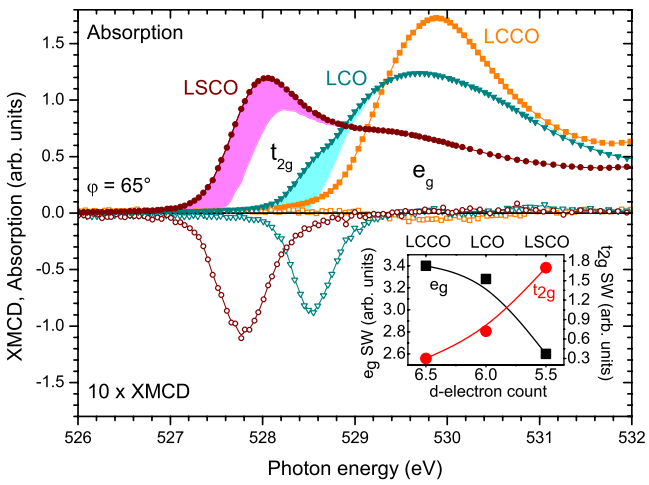

FIG. 7. (Color online) O *K* SXMCD and absorption of LCO, LSCO, and LCCO taken at 20 K. The absorption intensity is strongly doping dependent. A strong XMCD effect is found for LCO and LSCO while it is small for LCCO. The shaded areas in the absorption data exemplify that the SXMCD signal is limited to the t_{2g} range. Inset: spectral weight for e_g and t_{2g} levels in a simple ionic model (for details, see text).

configurations at the O K edge, Co-O hybridizations and charge-transfer effects have to be taken into account. For Co^{3+} and Co^{4+} IS states their respective $\alpha|d^5\rangle+\beta|d^6\underline{L}\rangle$ and $\alpha'|d^6\rangle+\beta'|d^7\underline{L}\rangle$ configurations are relevant only if the prefactors β and β' are significant.[5] More specifically, the intermediate-spin states are possible only if the doped holes have a relatively high probability to be found on the O sites. To further study this aspect we compare for LCCO, LCO, and LSCO the total O K SW in the energy range depicted in Fig. 7 (526–532 eV): the integration yields 3.43 arb. units eV for LCCO, 3.21 arb. units eV for LCO, and 3.08 arb. units eV for LSCO. For electron-doped LCCO IS states can be ruled out (see discussion of Figs. 3 and 5). When going to LCO and LSCO, the hole count on the Co-O bonds has to grow concurrently with the increase in the formal valence from +2.7 (LCCO) to +3 (LCO) and to +3.3 (LSCO). In contrast, the number of holes on the O sites, reflected by the total O K SW, decreases continuously despite an increasing Co valence. This finding clearly shows that the holes mainly reside on the Co sites (not at the O sites), rendering the β factors small, and thereby demonstrating once again that IS states are not relevant in LCO and LSCO thin-film samples.

The O K SXMCD spectra in the lower part of Fig. 7 show a strong negative peak ($\approx$7% of the absorption signal) in the t_{2g} area for LSCO and LCO and a very small one (within the error of the experiment) in the e_g area for LCCO. Due to the absence of spin-orbit splitting for an O 1s core hole, the O K edge SXMCD spectra display merely the orbital moment but are insensitive to the spin moment. Accordingly, for LSCO the t_{2g} feature reflects the transfer of a t_{2g} electron's orbital moment from the Co to the O site concomitant with the double exchange between Co^{3+} HS and Co^{4+} HS states [see also the sketch of the spin states in Fig. 8(a)]. The double-exchange mechanism is strongly supported by the metallic characteristics of LSCO.[55] Corresponding to the K-edge sum rule,[26,56] the orbital moment at the oxygen site, m_{orb}(O 2p), is given by

$$m_{\mathrm{orb}}(\mathrm{O}\ 2p) = -\frac{2}{3}\frac{\Delta A_K}{A_K} n_h^{\mathrm{O}}, \tag{7}$$

where m_{orb}(O 2p) is in units of μ_B/atom, n_h^{O} is the number of O 2p holes, and ΔA_K and A_K are the XMCD and XAS intensities integrated over the K edge. Usually it is difficult to extract orbital moments from this sum rule since the number of contributing O 2p holes is not known. Using the value of $n_h^{\mathrm{O}} \approx 0.15$ obtained from our multiplet simulations, m_{orb}(O 2p) can be estimated to be around 1.5×10^{-3} μ_B/O and, thus, one order of magnitude smaller than the orbital moment on the Co site. Independently of the size of the orbital moment induced on the O site, the negative integrated O K SXMCD signal, ΔA_K, already shows that m_{orb}(O 2p)$>$0. Since according to Eqs. (1) and (2) both m_{orb}(Co 3d) and m_{spin}(Co 3d) have positive sign as well, the O 2p orbital moment is parallel to the Co 3d spin and orbital moment. Similar results are found for polycrystalline $La_{1-x}Sr_xCoO_3$ samples where this finding was interpreted as evidence for holes in the t_{2g} states.[57] The situation is, however, quite different for $La_{1-x}Sr_xMnO_3$ where the orbital moments on O and Mn sites are antiparallel and where (driven by the e_g double exchange) the moment is directly transferred from the O 2p to the Mn e_g states.[58] It might be speculated that, in addition to the $t_{2g}$$Co^{3+}$ HS/Co^{4+} HS double exchange, electron transport or even band formation might also be possible in LSCO films by e_g electron hopping between Co^{3+} HS/Co^{4+} HS sites and the Co^{3+} LS ions. If such e_g electron-hopping processes were present the question may arise why they do not contribute to the SXMCD signal of the sample in Fig. 7. The suppression of the e_g SXMCD SW, however, can be understood in terms of an orbital-moment quenching of the e_g states as a consequence of the crystal-field symmetry and/or of the strongly itinerant character of the charge carriers.

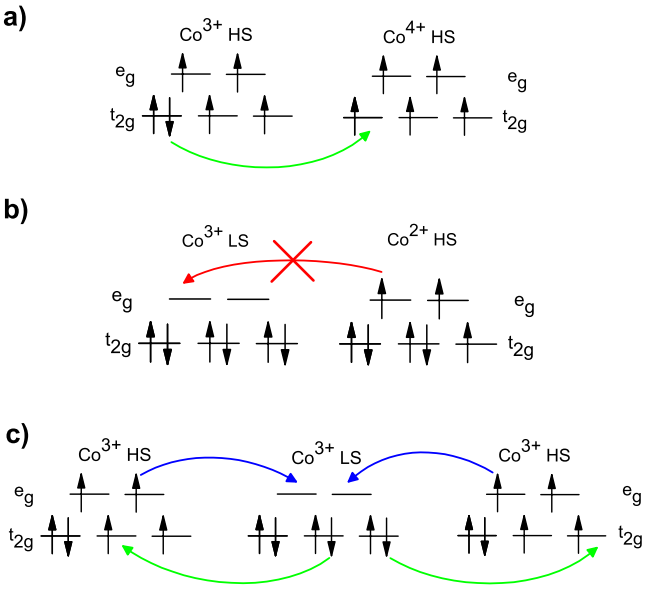

FIG. 8. (Color online) Scheme showing the relevant hopping process for (a) LSCO, (b) LCCO, and (c) LCO. (a) For the t_{2g} double exchange in LSCO an electron moves from a Co^{3+} HS site to a Co^{4+} HS neighbor. (b) For LCCO the spin blockade inhibits the transfer of an electron from the Co^{2+} HS to the Co^{3+} LS site. (c) For strained LCO correlated t_{2g} and e_g hopping processes between Co^{3+} LS and Co^{3+} HS neighbors lead to a ferromagnetic superexchange. Due to the correlated hopping of t_{2g} and e_g electrons, spin states are interchanged without a net transfer of charge. In the sketch, only the local t_{2g} and e_g hopping processes for the transformation of a Co^{3+} LS into a Co^{3+} HS ion are considered (Refs. 59 and 60).

In the case of LCCO the vanishing O K SXMCD SW demonstrates that both the t_{2g} and the e_g electrons are localized due to the spin blockade and do not induce a magnetic moment at the O site by hopping [see also the sketch of the spin states in Fig. 8(b)]. This finding is consistent with the insulating behavior of the samples. Further investigations with different Co^{2+}/Co^{3+} ratios will have to determine how the ferromagnetic ordering of the Co^{2+} HS states evolves. Similarly to epitaxial LCO and LSCO, percolationlike effects might play an important role for the ferromagnetism in this system.

For strained LCO, finally, the SXMCD spectrum shows a negative peak similar to LSCO but with slightly smaller in-

tensity. The peak is shifted by ≈0.8 eV to higher energies but still resides in the t_{2g} range. The apparent resemblance of the two features suggests a common origin. Furthermore, also for LCO $m_{orb}(O\ 2p)>0$, $m_{orb}(Co\ 3d)>0$, and $m_{spin}(Co\ 3d)>0$, i.e., the O $2p$ orbital moment is parallel to the Co $3d$ spin and orbital moment. Yet the double exchange found in the case of LSCO can be ruled out for LCO since all Co ions have the same valence of +3 and merely differ in their spin state. Ferromagnetism in epitaxial LCO films is, thus, established via superexchange where the spin and orbital moments of t_{2g} electrons "fluctuate" on Co^{3+} HS-O-Co^{3+} LS bonds [see also the sketch of the spin states in Fig. 8(c)]. In such a configuration fluctuation, Co^{3+} HS and Co^{3+} LS states are interchanged without a net transfer of charge.[52,59] Then the close similarity of the spectral shape of the t_{2g} peak in LSCO and LCO arises from the fact that in both systems an electron hops between t_{2g} levels on neighboring Co sites (via O $2p$ states). Interestingly, for a configuration fluctuation the charge transfer of the t_{2g} electrons is counterbalanced by the hopping of the e_g electrons between the corresponding Co neighbors [see sketch in Fig. 8(c)]. Similarly to the situation for LSCO, however, the spectral weight of the e_g levels does not contribute to the SXMCD signal (see Fig. 7). This finding suggests that for LCO the orbital moment of the e_g states is again quenched either by the crystal field or as a consequence of the itinerancy of the charge carriers.[60]

IV. SUMMARY AND CONCLUSIONS

To shed more light on the ferromagnetic mechanism of the cobaltates, NEXAFS and SXMCD measurements were performed on epitaxial $LaCoO_3$, on electron-doped $La_{0.7}Ce_{0.3}CoO_3$, and on hole-doped $La_{0.7}Sr_{0.3}CoO_3$ thin films. The spin and orbital moments were determined for the samples using the established sum rules and were corroborated by magnetometry investigations.

Our NEXAFS and SXMCD measurements result in the following picture for the spin degree of freedom in $La_{1-x}A_xCoO_3$ thin films: for $LaCoO_3$, 64% of the Co^{3+} ions are found to be in a low-spin state and 36% in a high-spin configuration. Superexchange between Co^{3+} high-spin and Co^{3+} low-spin ions where the spin and orbital moments of t_{2g} electrons fluctuate on Co^{3+} HS-O-Co^{3+} LS bonds is responsible for the ferromagnetism in epitaxial $LaCoO_3$. The spectroscopic data of the epitaxial films are consistent with a configuration fluctuation model. Percolationlike effects of high-spin/low-spin pairs in a low-spin matrix seem to cause a reduced spin moment of ≈0.8 μ_B/Co. Furthermore, the data reveal a strong magnetic anisotropy with the spin and orbital moments predominantly lying within the film plane.

For electron-doped $La_{0.7}Ce_{0.3}CoO_3$ the anisotropy is moderate. Nevertheless, the direction of the spin and orbital moments still resides preferably within the film plane. From the multiplet calculations and the Co $L_{2,3}$ NEXAFS spectra a 30% Co^{2+} HS/70% Co^{3+} LS configuration is found. The present work establishes that an insulating spin blockade between Co^{3+} low-spin and Co^{2+} high-spin configurations occurs not only in layered systems like $La_{1.5}Sr_{0.5}CoO_4$ and $HoBaCo_2O_{5.5}$ but also in electron-doped perovskite cobaltates. Further investigations with different Co^{2+}/Co^{3+} ratios will have to determine how the ferromagnetic ordering of the Co^{2+} high-spin states evolves.

Finally, in the case of $La_{0.7}Sr_{0.3}CoO_3$ a mixture of about 40% Co^{3+} HS, 30% Co^{3+} LS, and 30% Co^{4+} HS is inferred from the multiplet simulations. A strong magnetic anisotropy with the spin and orbital moments essentially oriented within the film plane is observed for $La_{0.7}Sr_{0.3}CoO_3$. The magnetic moments result from t_{2g} double exchange between high-spin Co^{3+} and high-spin Co^{4+} states. Similar to strained $LaCoO_3$, the reduced spin moment of ≈0.9 μ_B/Co found for $La_{0.7}Sr_{0.3}CoO_3$ in the spectroscopic and in the magnetometry experiments can again be ascribed to percolationlike effects.

Taken together, the current study gives a natural explanation for the strong discrepancy found for the Curie temperature between the 30% electron-doped ($T_C \approx 23$ K) and the 30% hole-doped ($T_C \approx 194$ K) perovskite cobaltate. Moreover, the NEXAFS and SXMCD investigations at both Co L and O K edges did not give any indication for Co^{3+} and Co^{4+} intermediate-spin states throughout the complete doping series.

ACKNOWLEDGMENTS

We are indebted to B. Scheerer for his excellent technical support. We greatly appreciate fruitful discussions with E. Arac, T. Tietze, E. Goering, and F. M. F. de Groot. We gratefully acknowledge the Max-Planck Institute for Metals Research Stuttgart for use of their SXMCD end station at WERA and the ANKA Ångströmquelle Karlsruhe for the provision of beamtime. Part of this work was supported by the German Science Foundation (DFG) in the framework of the DFG Research Unit 960 "Quantum Phase Transitions."

*Corresponding author. michael.merz@kit.edu

[1] K. Takada, H. Sakurai, E. Takayama-Muromachi, F. Izumi, R. A. Dilanian, and T. Sasaki, Nature (London) **422**, 53 (2003).

[2] C. Martin, A. Maignan, D. Pelloquin, N. Nguyen, and B. Raveau, Appl. Phys. Lett. **71**, 1421 (1997).

[3] T. Vogt, P. M. Woodward, P. Karen, B. A. Hunter, P. Henning, and A. R. Moodenbaugh, Phys. Rev. Lett. **84**, 2969 (2000).

[4] S. K. Kwon, J. H. Park, and B. I. Min, Phys. Rev. B **62**, R14637 (2000).

[5] M. A. Korotin, S. Y. Ezhov, I. V. Solovyev, V. I. Anisimov, D. I. Khomskii, and G. A. Sawatzky, Phys. Rev. B **54**, 5309 (1996).

[6] T. Saitoh, T. Mizokawa, A. Fujimori, M. Abbate, Y. Takeda, and M. Takano, Phys. Rev. B **55**, 4257 (1997).

[7] C. Zobel, M. Kriener, D. Bruns, J. Baier, M. Grüninger, T. Lorenz, P. Reutler, and A. Revcolevschi, Phys. Rev. B **66**, 020402 (2002).

[8] P. Ravindran, H. Fjellvåg, A. Kjekshus, P. Blaha, K. Schwarz, and J. Luitz, J. Appl. Phys. **91**, 291 (2002).
[9] T. Saitoh, T. Mizokawa, A. Fujimori, M. Abbate, Y. Takeda, and M. Takano, Phys. Rev. B **56**, 1290 (1997).
[10] G. Vankó, J.-P. Rueff, A. Mattila, Z. Németh, and A. Shukla, Phys. Rev. B **73**, 024424 (2006).
[11] S. Stølen, F. Grønvold, H. Brinks, T. Atake, and H. Mori, Phys. Rev. B **55**, 14103 (1997).
[12] G. Maris, Y. Ren, V. Volotchaev, C. Zobel, T. Lorenz, and T. T. M. Palstra, Phys. Rev. B **67**, 224423 (2003).
[13] M. Zhuang, W. Zhang, and N. Ming, Phys. Rev. B **57**, 10705 (1998).
[14] S. Noguchi, S. Kawamata, K. Okuda, H. Nojiri, and M. Motokawa, Phys. Rev. B **66**, 094404 (2002).
[15] Z. Ropka and R. J. Radwanski, Phys. Rev. B **67**, 172401 (2003).
[16] M. W. Haverkort *et al.*, Phys. Rev. Lett. **97**, 176405 (2006).
[17] N. Sundaram, Y. Jiang, I. E. Anderson, D. P. Belanger, C. H. Booth, F. Bridges, J. F. Mitchell, T. Proffen, and H. Zheng, Phys. Rev. Lett. **102**, 026401 (2009).
[18] J. M. Rondinelli and N. A. Spaldin, Phys. Rev. B **79**, 054409 (2009).
[19] K. Gupta and P. Mahadevan, Phys. Rev. B **79**, 020406 (2009).
[20] R. Eder, Phys. Rev. B **81**, 035101 (2010).
[21] D. Fuchs, C. Pinta, T. Schwarz, P. Schweiss, P. Nagel, S. Schuppler, R. Schneider, M. Merz, G. Roth, and H. v. Löhneysen, Phys. Rev. B **75**, 144402 (2007).
[22] C. Pinta, D. Fuchs, M. Merz, M. Wissinger, E. Arac, H. v. Löhneysen, A. Samartsev, P. Nagel, and S. Schuppler, Phys. Rev. B **78**, 174402 (2008).
[23] D. Fuchs, P. Schweiss, P. Adelmann, T. Schwarz, and R. Schneider, Phys. Rev. B **72**, 014466 (2005).
[24] D. Fuchs, T. Schwarz, O. Morán, P. Schweiss, and R. Schneider, Phys. Rev. B **71**, 092406 (2005).
[25] T. Yanagida, Y. Saitoh, Y. Takeda, A. Fujimori, H. Tanaka, and T. Kawai, Phys. Rev. B **79**, 132405 (2009).
[26] B. T. Thole, P. Carra, F. Sette, and G. van der Laan, Phys. Rev. Lett. **68**, 1943 (1992).
[27] P. Carra, B. T. Thole, M. Altarelli, and X. Wang, Phys. Rev. Lett. **70**, 694 (1993).
[28] M. Altarelli, Phys. Rev. B **47**, 597 (1993).
[29] D. Fuchs, E. Arac, C. Pinta, S. Schuppler, R. Schneider, and H. v. Löhneysen, Phys. Rev. B **77**, 014434 (2008).
[30] J. Stöhr and H. König, Phys. Rev. Lett. **75**, 3748 (1995).
[31] F. Reinert, P. Steiner, S. Hüfner, H. Schmitt, J. Fink, M. Knupfer, P. Sandl, and E. Bertel, Z. Phys. B: Condens. Matter **97**, 83 (1995).
[32] The error limits of each point are smaller than its symbol size.
[33] Z. Hu *et al.*, Phys. Rev. Lett. **92**, 207402 (2004).
[34] R. Nakajima, J. Stöhr, and Y. U. Idzerda, Phys. Rev. B **59**, 6421 (1999).
[35] S. Gota, M. Gautier-Soyer, and M. Sacchi, Phys. Rev. B **62**, 4187 (2000).
[36] B. T. Thole and G. van der Laan, Europhys. Lett. **4**, 1083 (1987).
[37] B. T. Thole, G. van der Laan, and P. H. Butler, Chem. Phys. Lett. **149**, 295 (1988).
[38] G. van der Laan, B. T. Thole, G. A. Sawatzky, and M. Verdaguer, Phys. Rev. B **37**, 6587 (1988).
[39] F. M. F. de Groot, J. C. Fuggle, B. T. Thole, and G. A. Sawatzky, Phys. Rev. B **42**, 5459 (1990).
[40] F. M. F. de Groot, J. Electron Spectrosc. Relat. Phenom. **62**, 111 (1993).
[41] F. M. F. de Groot, Coord. Chem. Rev. **249**, 31 (2005).
[42] M. Abbate, J. C. Fuggle, A. Fujimori, L. H. Tjeng, C. T. Chen, R. Potze, G. A. Sawatzky, H. Eisaki, and S. Uchida, Phys. Rev. B **47**, 16124 (1993).
[43] Z. Hu *et al.*, J. Alloys Compd. **343**, 5 (2002).
[44] C. F. Chang *et al.*, Phys. Rev. Lett. **102**, 116401 (2009).
[45] R. H. Potze, G. A. Sawatzky, and M. Abbate, Phys. Rev. B **51**, 11501 (1995).
[46] D. Weller, J. Stöhr, R. Nakajima, A. Carl, M. G. Samant, C. Chappert, R. Mégy, P. Beauvillain, P. Veillet, and G. A. Held, Phys. Rev. Lett. **75**, 3752 (1995).
[47] C. T. Chen, Y. U. Idzerda, H.-J. Lin, N. V. Smith, G. Meigs, E. Chaban, G. H. Ho, E. Pellegrin, and F. Sette, Phys. Rev. Lett. **75**, 152 (1995).
[48] The general robustness of sum rules and their application for TM compounds is discussed in C. Piamonteze, P. Miedema, and F. M. F. de Groot, Phys. Rev. B **80**, 184410 (2009).
[49] Y. Teramura, A. Tanaka, and T. Jo, J. Phys. Soc. Jpn. **65**, 1053 (1996).
[50] P. Bruno, Phys. Rev. B **39**, 865 (1989).
[51] A. Maignan, V. Caignaert, B. Raveau, D. Khomskii, and G. Sawatzky, Phys. Rev. Lett. **93**, 026401 (2004).
[52] M. A. Señarís-Rodríguez and J. B. Goodenough, J. Solid State Chem. **118**, 323 (1995).
[53] R. Caciuffo, D. Rinaldi, G. Barucca, J. Mira, J. Rivas, M. A. Señarís-Rodríguez, P. G. Radaelli, D. Fiorani, and J. B. Goodenough, Phys. Rev. B **59**, 1068 (1999).
[54] We note that the multiplet simulations at the Co L_3 and L_2 edges illustrated above already indicate that the IS configurations cannot be a significant species in the systems under study here.
[55] H. M. Aarbogh, J. Wu, L. Wang, H. Zheng, J. F. Mitchell, and C. Leighton, Phys. Rev. B **74**, 134408 (2006).
[56] J.-i. Igarashi and K. Hirai, Phys. Rev. B **50**, 17820 (1994).
[57] J. Okamoto *et al.*, Phys. Rev. B **62**, 4455 (2000).
[58] T. Koide, H. Miyauchi, J. Okamoto, T. Shidara, T. Sekine, T. Saitoh, A. Fujimori, H. Fukutani, M. Takano, and Y. Takeda, Phys. Rev. Lett. **87**, 246404 (2001).
[59] The complete picture of the configuration fluctuation model is outlined in Ref. 52: "in a configuration fluctuation, the Co^{3+} LS ions transfer two t_{2g} electrons equally to each of the six neighboring Co^{3+} HS ions and a Co^{3+} HS ion transfers back two e_g electrons equally to each of the six neighboring Co^{3+} LS ions, to give no net transfer of charge but an interchange of spin states."
[60] Alternatively, the ferromagnetism in strained LCO might be explained in terms of a ferromagnetic superexchange via virtual t_{2g} hopping processes between Co^{3+} LS and Co^{3+} HS neighbors.